Int J Clin Exp Pathol 2015;8(7):7849-7858
www.ijcep.com /ISSN:1936-2625/IJCEP0010454

Original Article

Myelin ultrastructure of sciatic nerve in rat experimental autoimmune neuritis model and its correlation with associated protein expression

Xiao-Jing Yuan[1,3], Yu-Jun Wei[2], Qiang Ao[2], Kai Gong[4], Jian-Yong Wang[2], Qiang-San Sun[1], Ling Zhang[5], Zun-Cheng Zheng[3], Lin Chen[4]

[1]Department of Rehabilitation, The Second Hospital, Shandong University, Shan Dong, China; [2]Department of Tissue Engineering, China Medical University, Shenyang, Liaoning, China; [3]Taian City Central Hospital, Shan Dong, China; [4]Institute of Neurological Disorders, Yuquan Hospital, Tsinghua University, Beijing, China; [5]Department of Ophthalmology, UCSF, USA

Received May 20, 2015; Accepted June 28, 2015; Epub July 1, 2015; Published July 15, 2015

Abstract: To explore the relationship of peripheral nerve ultrastructure and its associated protein expression in experimental autoimmune neuritis (EAN). EAN was established in Lewis rats using an emulsified mixture of P0 peptide 180-199, Mycobacterium tuberculosis, and incomplete Freund's adjuvant. Rats immunized with saline solution were used as a control group. Sciatic nerve ultrastructure and immunofluorescence histopathology were measured at the neuromuscular severity peak on day 18 post-induction. Cell-specific protein markers were used for immunofluorescence histopathology staining to characterize sciatic nerve cells: CD3 (T cell), Iba-1 (microglia), S100 (myelin), and neurofilament 200 (axon). The results showed that swelling of the myelin lamellae, vesicular disorganization, separation of the myelin lamellae, and an attenuation or disappearance of the axon were observed by transmission electron microscopy in the EAN group. CD3 and Iba-1 increased significantly in the structures characterized by separation or swelling of the myelin lamellae, and increased slightly in the structures characterized by vesicular of the myelin lamellae, S100 decreased in the structures characterized by vesicular disorganization or separation of the myelin lamellae. And neurofilament 200 decreased in the structures characterized by separation of the myelin lamellae. Furthermore, we found that Iba1 were positive in the myelin sheath, and overlapped with S100, which significantly indicated that Schwann cells played as macrophage-like cells during the disease progression of ENA. Our findings may be a significant supplement for the knowledge of EAN model, and may offer a novel sight on the treatment of Guillain-Barré syndrome.

Keywords: Experimental autoimmune neuritis (EAN), sciatic nerve, myelin ultrastructure, immunofluorescence histopathology, protein marker

Introduction

Guillain-Barré syndrome (GBS) is an acquired immune-mediated peripheral neuropathy. The most frequent form of GBS in Western countries is acute inflammatory demyelinating polyneuropathy (AIDP), which is characterized clinically by acute/subacute ascending paralysis and hyporeflexia with variable sensory involvement [1, 2]. In the Western Balkans, the most common reported pathologies of GBS were demyelinating (62%) and axonal (12%) [3]. This disease is characterized by an autoimmune reaction directed against specific components of the peripheral nerves with involvement of both humoral and cellular factors [4, 5].

Experimental autoimmune neuritis (EAN) is a useful animal model for studying the pathogenesis and treatment of GBS. In 1955, Waksman and Adams made the first rabbit model of human GBS [6]. Thereafter, researchers used purified peripheral nerve tissue, purified myelin protein ingredients, synthetic peptides, or antigen-specific autoimmune T cells injected intravenously into mice to induce various susceptible animal models of GBS [7, 8]. The most common model uses Lewis rats that have been immunized with peripheral nerve homogenate, myelin protein, or a synthetic peptide, such as P0 180-199, emulsified in Freund's adjuvant [9].

Recently, studies of EAN electrophysiology, histology, immune mechanisms, and therapeutic drug use have been reported [10-15]. Like GBS, EAN is also characterized by an autoimmune reaction directed against specific components of the peripheral nerves with involvement of both humoral and cellular factors [10, 11]. The immune responses in EAN are complex and involve T-cells, cytokines, chemokines, macrophages, adhesion molecules, the blood-nerve barrier, and humoral immune factors [12, 13]. Despite decades of research, studies investigating the microstructure characteristics of EAN are comparatively rare. In 1975, Allt used an EAN rabbit model to study the pathological changes in peripheral nerves by electron microscopy and found that there are two kinds of myelin changes: a vesicular disorganization of myelin lamellae and a separation of myelin lamellae [14]. However, there are no further detailed reports on the microstructure in EAN. To elucidate the pathologic mechanisms of peripheral nerve inflammation that may be extrapolated to human disease, it is important to observe the microstructure of peripheral nerves in EAN and determine the correlation between the peripheral nerve ultrastructure and its associated protein expression. In EAN, pathological changes are the most obvious in the sciatic nerve and lumbar nerve root [15], so in this study, we examined the ultrastructure and immunofluorescence histopathology of the sciatic nerve.

Materials and methods

Animals and reagents

Healthy female Lewis rats, 6-8 weeks old, weighing 135-145 g, bought from Vital River Corporation (Beijing, China) were housed and maintained under environmentally controlled conditions in a 12-hour light/dark cycle with standard food and water by the Tsinghua University Center of Biomedical Analysis. All experimental drugs were used at the lowest possible effective dose, and animal suffering was reduced as much as possible. The experiments were approved by the Tsinghua University animal ethics committee.

The P0 peptide 180-199 (SSKRGRQTPVLYAMLDHSRS) was synthesized by Anhui Boxing Biotechnology Company. Incomplete Freund's adjuvant (IFA) was from Sigma, United States. Mycobacterium tuberculosis (H37Ra) was obtained from Difco, United States.

EAN induction and clinical score

Lewis rats (n = 10) were immunized in both hind footpads with 200 μl inoculum containing 200 μg P0 peptide 180-199, 2 mg H37Ra in 100 μl saline and 100 μl IFA. Control group rats (n = 10) received the same treatment with the same dose of saline solution. The day of model induction was recorded as day 0.

All rats were weighed and scored daily until day 42 post-immunization (p.i.). Score criteria were as follows: 0, normal; 1, flaccid or dragging tail; 2, mild paraparesis; 3, moderate paraparesis; 4, severe paraparesis; and 5, severe tetraparesis [13, 14]. Symptoms were scored by plus or minus 0.5 points, according to conditions.

Electrophysiology

Electrophysiology studies were conducted on day 18 p.i. using a multi-channel physiological signal acquisition processing system (RM6240). Five animals from each group were randomly selected. They were weighed and anesthetized with an intraperitoneal injection of 0.35 mg/100 g of 10% chloral hydrate, and fixed on the operating platform. Sciatic nerves were separated layer by layer. To assess sciatic nerve motor conduction, the sciatic nerve was stimulated through paired electrodes at the distal (recording electrode) and the proximal (stimulating electrode) ends of the sciatic nerve. A reference electrode was placed at a point 1 cm away from the recording electrodes, between the stimulating electrode and the recording one.

The nerve was stimulated with 1.5 times the threshold at rectangular pulses, 0.1 ms in duration, and the amplitudes and latencies of the evoked compound nerve action potential (CNAP) were recorded from distal electrodes on the sciatic nerve. Motor conduction velocity (MCV) was calculated by dividing the distance between the recording and stimulating electrodes by the latency of the response [16]. The amplitude was calculated by measuring the distance from peak to peak valley of the bipolar compound action potential. Each stimulus was carried out 7-10 times. Each interval between the two stimuli was at least 5 s. The room temperature was set at 20 ± 0.5°C and body temperatures of the rats were kept at 37°C.

When the testing was completed, the animals were sacrificed, and the bilateral sciatic nerves and gastrocnemius were removed for histological analyses.

Light microscopy

Gastrocnemii were removed after the electrophysiology tests described above and fixed in 4% paraformaldehyde solution for 12 h, then put into 30% sucrose phosphate buffer for 1 d until they sunk to the bottom. Vertical sections 20 μm thick were cut on a freezing microtome. Hematoxylin and eosin (H&E) staining were performed, as described below, and the resulting sections were examined by light microscopy to evaluate bilaterality and induction of EAN pathologically.

H&E staining: The slides were brought to room temperature, placed in a glass chamber, and washed with running tap water to remove any remaining formaldehyde. To stain the nuclei dark, the slides were incubated with Mayer's hematoxylin solution for 5 minutes, followed by a 10-min wash. Acetic acid (1:100) was added to a 0.5% eosin solution, and the slides were incubated in this solution for 10 min to stain the fibers red. Then, the slides were washed three times with deionized water for 1 min each to remove excess eosin. Next, the slides were drained successively in 70% EtOH for 1 minute, 90% EtOH for 30 seconds, 100% EtOH for 30 seconds, and xylene for 30 seconds. The slides were mounted with 1-2 drops of a xylene-based mounting media, covered with cover slides, and then pressed under heavy weight for 10 min at room temperature. The slides were stored at room temperature until use.

Nerve ultrastructure visualization by transmission electron microscopy

For histological analysis, sciatic nerves were removed about 1 cm away from the sections used for the electrophysiology tests, and the nerve specimens were fixed with pre-cooled 2.5% glutaraldehyde in 0.1 M phosphate-buffered saline for 1-2 h and post-fixed in 1% osmium tetraoxide solution for 1 h. Then, they were dehydrated stepwise in increasing concentrations of ethanol and embedded in Epon 812 epoxy resin. The specimens were cut into ultrathin sections, 70 nm thick, and stained with lead citrate and uranyl acetate. They were examined by transmission electron microscopy (TEM; H-7650, Hitachi, Japan). The nerve specimens from the control group were used as a positive control for nerve histological analysis. The electron microscopy images from eight random fields of each nerve section were selected and analyzed by Image-Pro Plus software.

Immunofluorescence histopathology

The intact nerves were selected and removed after the electrophysiology tests on day 18 p.i., as discussed above, and then they were fixed in 4% paraformaldehyde solution for 12 h and put into 30% sucrose phosphate buffer for 1 d, until they sunk to the bottom. Cross sections, 20-30 μm thick, were cut on a freezing microtome.

Immunofluorescence chemical studies were performed using cell-specific markers to characterize the cells in the sciatic nerve: CD3 (T cell), Iba-1 (microglia), S100 (myelin), and neurofilament 200 (axon). Five unimmunized rats were also measured as controls. The following primary antibodies were used: rabbit anti-CD3 antibody (1:100; ABCAM, USA), rabbit anti-Iba-1 antibody (1:250; Wako Pure Chemical Industries, Ltd, Japan), mouse anti-S100 antibody (1:500; ABCAM, USA), and anti-neurofilament 200 antibody (1:80; Sigma, USA).

For secondary antibodies, goat anti-rabbit IgG (FITC) and goat anti-mouse IgG (TRITC) (Dako Japan) were used. Primary antibodies were incubated with the samples overnight at 4°C, and secondary antibodies were incubated with them for 1 hour at room temperature. After immunostaining, images were acquired with a laser confocal microscope (FV10i -oil, push around, Tokyo, Japan). The density of the stained cell surface area per unit area (photographed at 103, 203 objective lens magnification) were analyzed using Image J software (U.S. National Institutes of Health, Bethesda, MD, USA).

Statistical analysis

GraphPad Prism (GraphPad Software, San Diego, CA, USA) was used for statistical analysis and graph generation. A Mann-Whitney U test was used to compare threshold, stained maker density, and stained marker surface area between EAN model rats and normal control rats. Statistical significance was defined as $P < 0.05$ in all data analyses.

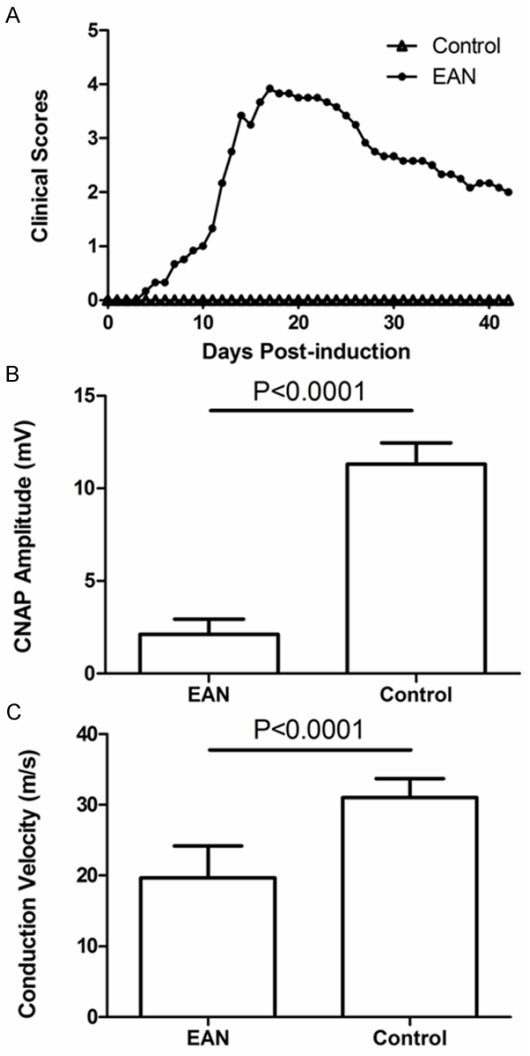

Figure 1. (A) Clinical scores of the EAN model and control rats during the course of the experiment and (B, C) electrophysiology on day 18 p.i. during the maximal mean clinical score. (A) Rats were immunized with 200 μg P0 180-199 emulsified in IFA and H37Ra (EAN, n = 10) or with saline (Control, n = 10). The clinical score was measured every day for both groups. Data are expressed as mean ± SEM. Similar results were obtained in two independent experiments. (B) The sciatic nerve compound nerve action potential (CNAP) amplitude and (C) the conduction velocity were measured for each group. Data are expressed as mean ± SEM. $P < 0.0001$ compared with control. Similar results were obtained in two independent experiments.

Results

Progress of illness, clinical scores and electrophysiology

On day 1 p.i., all rats in the EAN model group began to display different clinical symptoms with varying degrees of severity, including depression and red and swollen feet. On day 7 p.i., the tail tonicity was lost in all experimental rats, which suggests that the EAN model was successfully established. With a rapid progression to maximal severity, the symptoms peaked on day 17-18 p.i. and included severe hindlimb paralysis accompanied by skin lesions in the foot pads. The symptoms lasted about 7-10 days, and then normal function was gradually restored. The animals remained stable through day 42 p.i. (**Figure 1A**). Two rats died over the course of the experiment, one each on days 12 and 24 p.i.

Based on the neuromuscular severity scores, the onset of EAN occurred at day 7 p.i. and the mean clinical score at that time was 0.67 ± 0.26. The peak clinical score was reached, on average, by day 17 p.i. and the maximal mean clinical score was 3.92 ± 0.2. Afterward, there was a gradual recovery, with residual weakness present, during which the mean clinical score was 2.00 ± 0.32. There was no appreciable neuromuscular weakness detected in the control rats ($P < 0.0001$) (**Figure 1A**).

On day 18 p.i., which was the peak of neuromuscular symptoms, the electrophysiology of five rats from each group was examined. The sciatic nerve CNAP (peak to peak) in the EAN group (2.12 ± 0.83 mV) was significantly lower than that in the control group (12.18 ± 1.71 mv; $P < 0.0001$) (**Figure 1B**). Similarly, the sciatic nerve conduction velocity in the EAN model group (19.69 ± 4.47 m/s) was significantly lower than that in the control group (30.98 ± 2.71 m/s; $P < 0.0001$) (**Figure 1C**).

Light microscopy histology

To examine the microstructure of the gastrocnemius, H&E were performed. In the H&E staining, the control group gastrocnemius myofibers had a polygonal shape with peripheral nuclei, intact sarcolemma, and non-fragmented sarcoplasm. The intact muscle tissue of the control group showed a homogenous fiber size distribution (**Figure 2A**). In contrast, the EAN model group gastrocnemius myofibers stained lighter than intact muscle fibers typically do and had an irregular shape and few nuclei. The muscle fibers in the EAN model group were atrophied and distributed unevenly (**Figure 2B**).

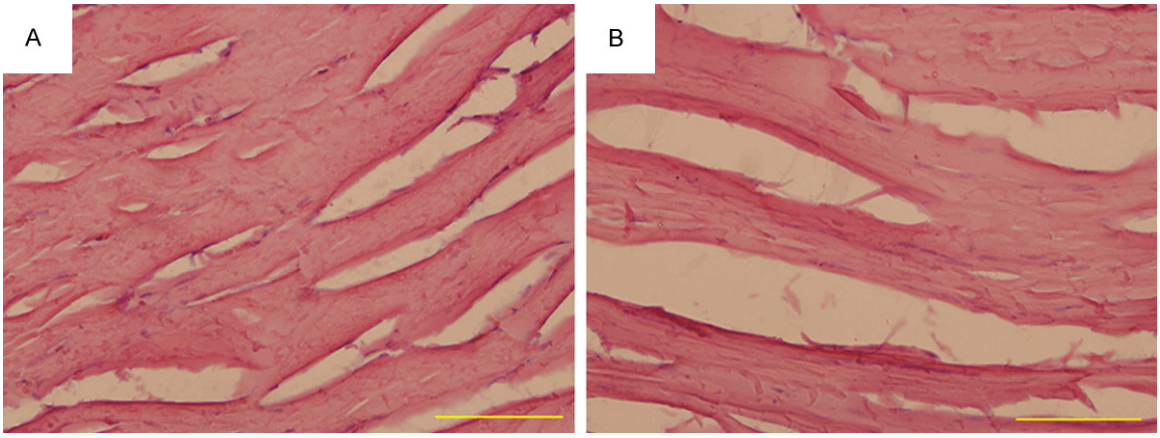

Figure 2. H&E staining of rat gastrocnemius myofibers on day 18 p.i. of (A) the control group and (B) the EAN model group (bar = 100 μm).

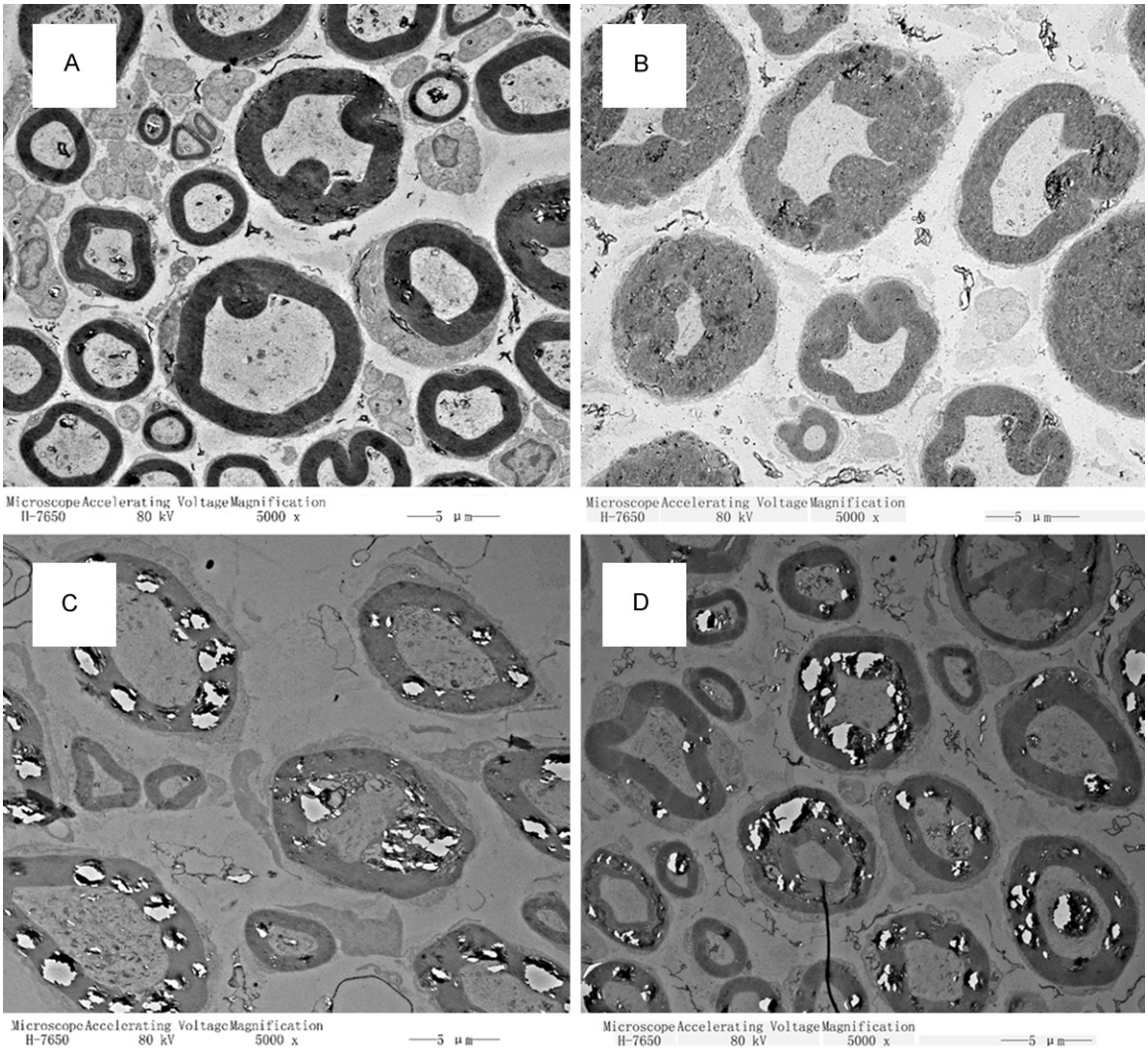

Figure 3. TEM microscopy of the sciatic nerves on day 18 p.i. Of (A) the control group and (B-D) the EAN model group. (B) swelling of the myelin lamellae, (C) vesicular disorganization, and (D) separation of the myelin lamellae were observed in the EAN group by using TEM (bar = 5 um).

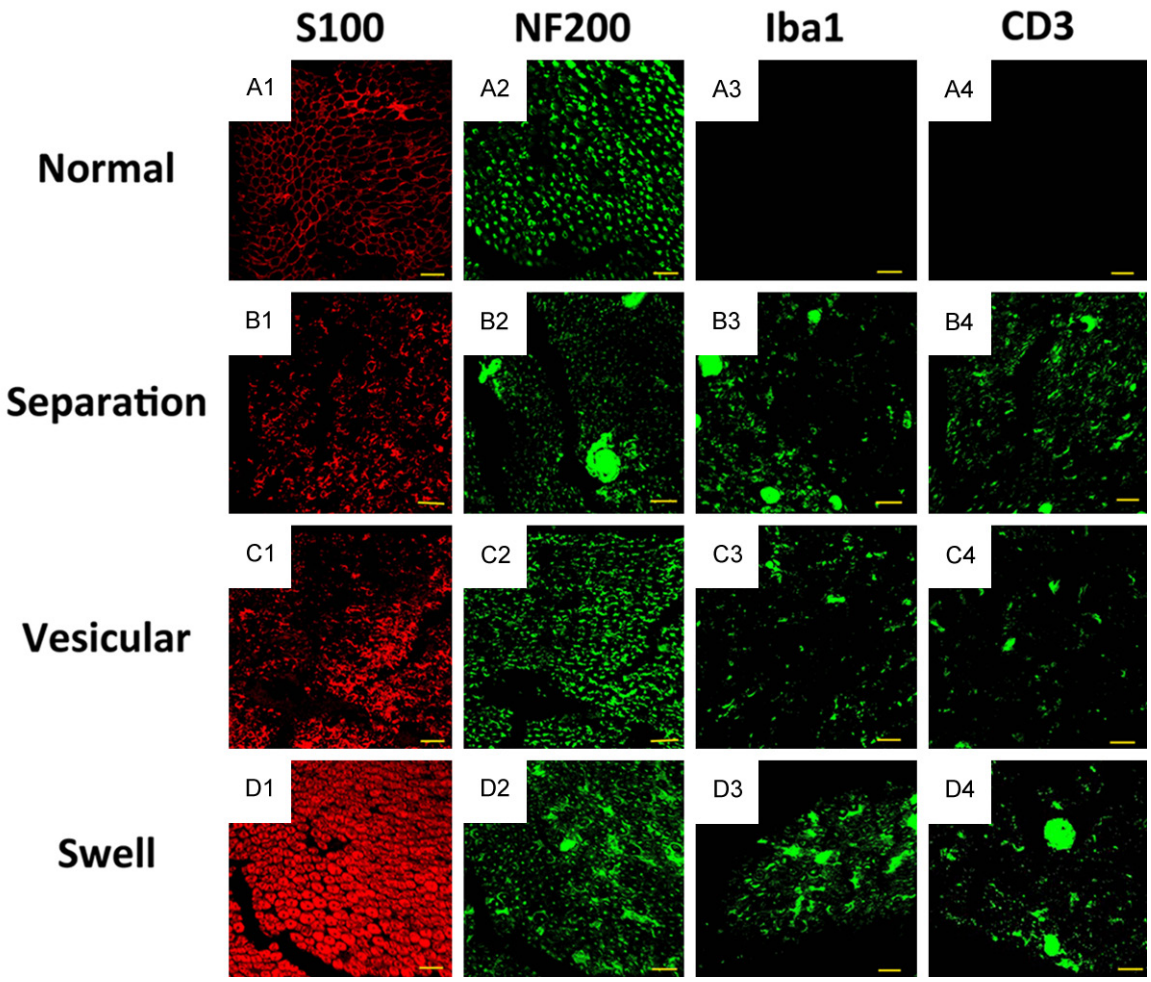

Figure 4. Immunofluorescent histology of the sciatic nerves in different TEM structures (A1-A4) in the control group rats and (B1-D4) in the EAN model group rats. Representative immunofluorescent histology images were shown staining with (A1-D1) S100, (A2-D2) NF200, (A3-D3) Iba1 or (A4-D4) CD3. (bar = 20 μm).

Correlation between sciatic nerve ultrastructure and immuofluorescence histopathology

The ultrastructure of the sciatic nerves was visualized with TEM and immunofluorescence histopathology at the peak of neuromuscular severity on day 18 p.i. (**Figure 1**) to determine if there is a correlation between the ultrastructure and the histopathology in EAN. Using TEM, we saw normal structures in the nerve specimens from the control group rats, and we observed a swelling of the myelin lamellae, a vesicular disorganization and a separation of the myelin lamellae, and an attenuation or disappearance of the axon in samples from the EAN group (**Figure 3**). Immunohistochemistry also revealed an irregularity of the neuro myelin and axon in the EAN model group compared with the structures observed in the control group (**Figure 4**).

In specimens that showed the pathological changes of swollen, separated and hollowed myelin lamellae, the predominant cells that infiltrated the sciatic nerve were T cells (CD3) and microglia (Iba-1). This finding supports previous work demonstrating that EAN is pathogenetically characterized by an autoimmune reaction with the involvement of both humoral and cellular factors. In nerve specimens that displayed the pathological change of myelin lamellae separation in the absence of swelling, the marker proteins of S100 and NF200 decreased compared with the levels in the control group rats, which illustrates that myelin protein and axon protein were likely attacked by inflamma-

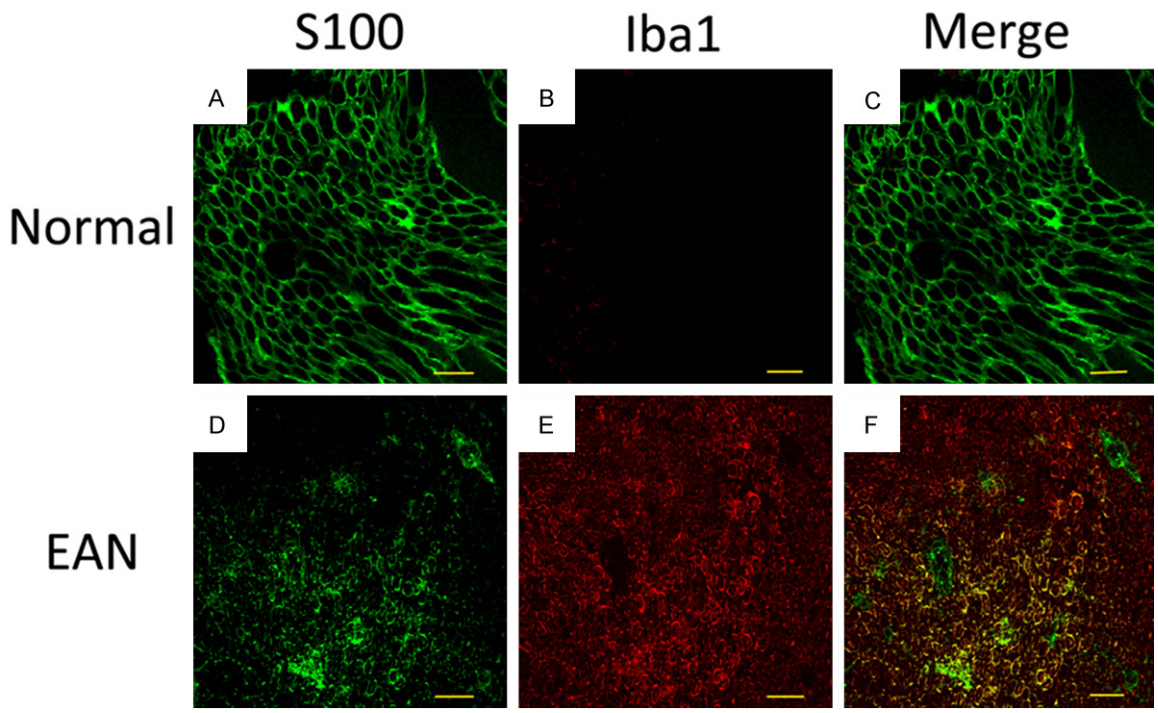

Figure 5. Immunofluorescent histology of the sciatic nerves on S100 (green) and Iba-1 (red) on day 18 p.i. (A-C) in the control group rats and (D-F) in the EAN model group rats. Iba-1 was expressed in the myelin sheath (E), like S100 (D), but was merged by S-100 (F). (bar = 20 μm).

tory cytokines, possibly by Iba1 and CD3 or other inflammatory cytokines. The specimens showing the pathological change of vesicular disorganization may be another progress of the disease, when inflammatory cells and factors have already been absorbed by a certain degree. Alternately, the myelin protein S100 in these samples may have been attacked by other inflammatory cytokines besides Iba1 and CD3 (**Figure 4**).

Immunofluorescence histopathology of S100 and Iba1

As presented in **Figure 5**, the number of S100-positive cells was significantly lower in the EAN group than the control group. The expression of Iba1 was significantly higher in EAN group than the control group. Moreover Iba1 were positive in the myelin sheath, and overlapped with S100, which significantly indicated that Schwann cells played as macrophage-like cells during the disease progression of ENA.

Discussion

In this experiment, Lewis female rats were successfully immunized in both hind footpads with 200 μg of P0 peptide 180-199, as in previous studies [8, 9]. The neuromuscular severity was observed by the single-blind method, and recorded by a grading method with six levels [17, 18]. On day 1 p.i., all rats in the EAN model group developed symptoms, including malaise, footpad swelling, weight loss, or reduced weight performance. By day 7 p.i., the tail tonicities were lost in all rats, implying the model was successfully established. On day 17-18 p.i., rat symptoms peaked. The systemic symptoms, such as malaise, on the first day after induction were related to the systemic immune responses that were caused by the immunogen, which are similar to non-specific syndromes of virus infection such as human GBS [19].

In the control group, the injected footpads had some localized mild redness after the saline injection that faded after 2-3 days, which matches the pathological process of purely local trauma. In contrast, swelling gradually increased after drug injection in the EAN model group, until the footpads of the rats festered. We speculate that this reaction corresponds to the local performance of a systemic autoimmune reaction as the neuromuscular severity

peaked. Although both groups of rats continued to gain weight over the course of the experiment, which is expected because of their age, the rats in the EAN model group weighed significantly less than those in the control group (**Figure 2**). The clinical scores of the rats in our experiment never reached the maximal five points (i.e., both arms and legs are weak), but most had four points, namely severe weakness in both hind legs, at their peak. This phenomenon may be related to the use of different inducers, rat species, and induction time points than previous studies. For example, Robin H. Xia used BPNM to induce EAN in 8-12-week-old SJL/J mice and found that symptoms peaked at an average score of 4.8 points on days 31-33 p.i. [16]. Additionally, rat symptom onset time and peak symptom time reflect individual differences.

As early as 1975, Allt studied the peripheral nerves of an EAN rabbit model by electron microscopy and found that there were two kinds of myelin sheath change: (1) a vesicular disorganization of the myelin lamellae and (2) a separation of the myelin lamellae [14]. In this experiment, when the neuromuscular severity of all rats peaked, we found through TEM that there are four different pathological manifestations of the sciatic nerve: (1) swelling of the myelin lamellae, (2) vesicular disorganization of the myelin lamellae, (3) separation of the myelin lamellae, and (4) attenuation or disappearance of the axon. The three kinds of myelin sheath changes corresponded to neuromuscular severities of 3.5 to 4 points, namely to severe paraparesis or slightly lighter than severe paraparesis, when rats were unable to walk, walked very slowly or walked slowly by using only one hind leg.

The myelin swelling in EAN was indirectly measured by immunohistochemistry in one previous study [18, 20], but to our knowledge, this is the first time that the pathological phenomena of the EAN sciatic nerve have been observed by electron microscopy. Our immunofluorescence results confirm that the inflammation leads to swelling of the myelin sheath cells and support the idea that EAN should be pathogenetically characterized by an autoimmune reaction with the involvement of both humoral and cellular factors. We found that Iba-1 (macrophage) and CD3 (T cell) staining significantly increased in the specimens that demonstrated swelling of the myelin lamellae. This observation may be the initial phase of EAN and could result from a failure of the S100 and NF200 levels to decrease.

The second EAN pathology we observed through TEM was a vesicular disorganization of the myelin lamellae. In these samples, NF200 staining did not significantly decrease compared with the levels in the control group. S100, which stains myelin, decreased significantly in these samples. Iba-1 (macrophage) and CD3 (T cell) staining increase slightly. This suggests that only myelin is under attack possibly by other inflammatory factors besides the two kinds of inflammatory factors investigated in this experiment. Further research is needed to explore the mechanisms responsible for this pathology.

We found a third kind of pathological change in myelin, specifically, a separation of the myelin lamellae. In this pathology, the outer structure of the myelin lamellae is complete, and does not display vesicular disorganization. This illustrates that a separation of the myelin lamellae and vesicular disorganization of the myelin lamellae might form from different pathologies and physiological procedures. S100 and NF200 staining were significantly decreased and Iba-1 (macrophage) and CD3 (T cell) staining were significantly increased in this pathology compared with their levels in the control group. These results suggest that inflammatory cytokines in the autoimmune reaction may attack the myelin and axon.

In our study, we also found that Iba1 were positive in the myelin sheath in the EAN group on day 18 p.i., and overlapped with S100, which significantly indicated that Schwann cells played as macrophage-like cells during the disease progression of ENA.

The sciatic nerve conduction velocity and CNAP amplitude slowed significantly in the EAN model group compared with those in the control group. Sciatic nerve conduction velocity is the ratio of the distance between the stimulating electrode and the recording electrode (unit: cm) to the initial latency time (unit: ms). This ratio implies the velocity conducted by the fastest nerve of a big nerve fiber bundle [21], and it is not restricted by the population of the neural axon. Therefore, this measurement partially reflects the degree of nerve demyelinating lesions.

Many factors affect the CNAP amplitude, the most important of which are temperature and axon number. In theory, the amplitude corresponds to the number of axons based on a temperature control. In brief, the higher the amplitude, the greater the number of axons there are in the sample [21]. This was confirmed by the fact that the model group had both significantly lower CNAP amplitudes, and fewer axon numbers per unit area visible in the electron microscopy images. The CNAP curve in the model group is not smooth, which may be related to tissue degeneration hyperplasia caused by inflammation between nerve axons that might lead to time differences in neuromuscular electrical conduction.

The gastrocnemius muscles dominated by sciatic nerves degenerated over the course of this experiment, because of the nerve lesions. The gastrocnemius myofibers in the EAN model group stained lighter than expected for intact muscle fibers and they had an irregular shape and few nuclei. Some myofibers were invaded by immune cells whose nuclei were stained by the hematoxylin. In addition to being the cause of nerve loss, this immune cell invasion is one of the reasons for the observed movement dysfunctions [22]. In this experiment, muscles degenerated significantly two weeks after induction, partially in response to the reduction in motion [22].

This study shows that Lewis rat EAN is a reliable model that recapitulates key clinical, electrophysiological, and pathologic features of GBS with a distinct disease severity peak. We found a correlation between the ultrastructure and the immunofluorescence histopathology in the peripheral nerves and fluorescent co-location of S100 and Iba1, which has furthered our understanding of the mechanisms pertinent to peripheral nerve demyelination and inflammation. These findings may accelerate the development of targeted, immune-specific therapies for GBS.

Acknowledgements

This work was supported by the National High Technology Research and Development Program of China ("863" Program, No. 2012-AA020905), the Chow Tai Fook Medical Research Special Fund (202836019-03) and the National Natural Science Foundation of China (81171143).

Disclosure of conflict of interest

None.

Address correspondence to: Drs. Qiang Ao and Yu-Jun Wei, Department of Tissue Engineering, China Medical University, Shenyang, Liaoning, China. E-mail: aoqiang@tsinghua.edu.cn (QA); weiyj501@tsinghua.edu.cn (YJW); Dr. Qiang-San Sun, Department of Rehabilitation, The Second Hospital, Shandong University, Jinan, Shandong, China. E-mail: sunqsan@126.com

References

[1] Winer JB. An update in Guillain-Barre syndrome. Autoimmune Dis 2014; 2014: 793024.

[2] Petratos S, Gonzales MF. Can antiglycolipid antibodies present in HIV-infected individuals induce immune demyelination? Neuropathology 2000; 20: 257-72.

[3] Peric S, Milosevic V, Berisavac I, Stojiljkovic O, Beslac-Bumbasirevic L, Marjanovic I, Djuric V, Djordjevic G, Rajic S, Cvijanovic M, Babic M, Dominovic A, Vujovic B, Cukic M, Petrovic M, Toncev G, Komatina N, Martic V, Lavrnic D. Clinical and epidemiological features of Guillain-Barré syndrome in the Western Balkans. J Peripher Nerv Syst 2014; 19: 317-21.

[4] Buus L, Tønnesen EK. Intensive therapy for patients with Guillian-Barré syndrome. Ugeskr Laeger 2014; 176 pii: V05120247.

[5] Talukder RK1, Sutradhar SR, Rahman KM, Uddin MJ, Akhter H. Guillian-Barre syndrome. Mymensingh Med J 2011; 20: 748-56.

[6] Goihman-Yahr M, Requena MA, Vallecalle-Suegart E, Convit J. Autoimmune disease and thalidomide. II. Adjuvant disease, experimental allergic encephalomyelitis and experimental allergic neuritis of the rat. Int J Leprosy 1974; 42: 266-75.

[7] Meyer zu Hörste G, Hartung HP, Kieseier BC. From bench to bedside-experimental rationale for immune-specific therapies in the inflamed peripheral nerve. Nat Clin Pract Neuro 2007; 3: 198-211.

[8] Xu H, Li XL, Yue LT, Li H, Zhang M, Wang S, Wang CC, Duan RS. Therapeutic potential of atorvastatin-modified dendritic cells in experimental autoimmune neuritis by decreased Th1/Th17 cytokines and up-regulated T regulatory cells and NKR-P1(+) cells. J Neuroimmunol 2014; 269: 28-37.

[9] Li H, Li XL, Zhang M, Xu H, Wang CC, Wang S, Duan RS. Berberine Ameliorates Experimental Autoimmune Neuritis by Suppressing both Cellular and Humoral Immunity. Scand J Immunol 2014; 79: 12-19.

[10] Lisak RP, Behan PO. Experimental autoimmune demyelinating diseases: experimental allergic encephalomyelitis and experimental allergic neuritis. Biomedicine 1975; 22: 81-87.
[11] Shin T, Ahn M, Matsumoto Y, Moon C. Mechanism of experimental autoimmune neuritis in Lewis rats: the dual role of macrophages. Histol Histopathol 2013; 28: 679-84.
[12] Zhang HL, Azimullah S, Zheng XY, Wang XK, Amir N, Mensah-Brown EP, Al Shamsi M, Shahin A, Press R, Zhu J, Adem A. IFN-γ deficiency exacerbates experimental autoimmune neuritis in mice despite a mitigated systemic Th1 immune response. J Neuroimmunol 2012; 246: 18-26.
[13] Zhang HL, Zheng XY, Zhu J. Th1/Th2/Th17/Treg cytokines in Guillain-Barré syndrome and experimental autoimmune neuritis. Cytokine Growth Factor Rev 2013; 24: 443-53.
[14] Allt G. The node of Ranvier in experimental allergic neuritis: an electron microscope study. J Neurocytol 1975; 4: 63-76.
[15] Izumo S, Linington C, Wekerle H, Meyermann R. Morphologic study on experimental allergic neutitis mediated by T cell line specific for bovine P2 protein in Lewis rats. Lab Invest 1985; 53: 209-18.
[16] Harvey GK, Pollard JD. Patterns of conduction impairment in experimental allergic neuritis. An electrophysiological and histological study. J Neurol Neurosurg Psychiatry 1992; 55: 909-15.
[17] Xia RH, Yosef N, Ubogu EE. Clinical, electrophysiological and pathologic correlations in a severe murine experimental autoimmune neuritis model of Guillain-Barré syndrome. J Neuroimmunol 2010; 219: 54-63.
[18] Matsunaga Y, Kezuka T, An X, Fujita K, Matsuyama N, Matsuda R, Usui Y, Yamakawa N, Kuroda M, Goto H. Visual Functional and Histopathological Correlation in Experimental Autoimmune Optic Neuritis. Invest Ophth Vis Sci 2012; 53: 6964-71.
[19] Asbury AK, Cornblath DR. Assessment of current diagnostic criteria for Guillain-Barré syndrome. Ann Neurol 1990; 27 Suppl: S21-24.
[20] Kajii M, Kobayashi F, Kashihara J, Yuuki T, Kubo Y, Nakae T, Kamizono A, Kuzumoto Y, Kusunoki S. Intravenous immunoglobulin preparation attenuates neurological signs in rat experimental autoimmune neuritis with the suppression of macrophage inflammatory protein -1α expression. J Neuroimmunol 2014; 266: 43-48.
[21] Water R. Frontera. Delisa Physical medicine and rehabilitation principles and practic. Beijing: People's Medical Publishing House; 2013. pp. 71.
[22] Calik MW, Shankarappa SA, Stubbs EB Jr. Forced-exercise attenuates experimental autoimmune neuritis. Neurochem Int 2012; 61: 141-145.